Evolutionary Dynamics of Complex Networks of HIV Drug-Resistant Strains: The Case of San Francisco

Robert J. Smith,[1]*† Justin T. Okano,[1]† James S. Kahn,[2] Erin N. Bodine,[1]‡ Sally Blower[1]§

Over the past two decades, HIV resistance to antiretroviral drugs (ARVs) has risen to high levels in the wealthier countries of the world, which are able to afford widespread treatment. We have gained insights into the evolution and transmission dynamics of ARV resistance by designing a biologically complex multistrain network model. With this model, we traced the evolutionary history of ARV resistance in San Francisco and predict its future dynamics. By using classification and regression trees, we identified the key immunologic, virologic, and treatment factors that increase ARV resistance. Our modeling shows that 60% of the currently circulating ARV-resistant strains in San Francisco are capable of causing self-sustaining epidemics, because each individual infected with one of these strains can cause, on average, more than one new resistant infection. It is possible that a new wave of ARV-resistant strains that pose a substantial threat to global public health is emerging.

HIV resistance to antiretroviral drugs (ARVs) is causing serious clinical and public health problems throughout the United States and Europe. HIV strains began to acquire resistance in 1987 when ARVs were introduced as therapies for HIV-infected individuals (*1*). Since then, a multitude of drug-resistant strains have evolved that differ considerably in their susceptibility to three major classes of ARVs: nucleoside reverse-transcriptase inhibitors (NRTIs), non-nucleoside reverse-transcriptase inhibitors (NNRTIs), and protease inhibitors (PIs). These drug-resistant strains are now being transmitted to individuals who have never received ARVs; that is, transmitted drug resistance (TDR) has arisen. TDR is reported to range between 8 and 22% in many HIV-infected communities in resource-rich countries, and if it continues to increase, the effectiveness of therapeutic regimens, as well as efforts to control the HIV pandemic, will be compromised. We have developed a theoretical model (the amplification cascade model) to help understand and predict the evolutionary dynamics of complex transmission networks composed of multiple ARV-resistant strains. We calibrated and parameterized the model to represent the HIV epidemic in San Francisco in the community of men who have sex with men (MSM), where TDR is already high (~13%) (*2*). The model was able to reproduce the observed dynamics and evolution of transmitted resistance in this city over the past 20 years. We used the model first to predict the future evolutionary dynamics of TDR. Next, we determined whether any of the currently circulating ARV-resistant strains are capable of generating self-sustaining epidemics. Third, we identified the key drivers that generate high levels of TDR. We also discuss here the implications of our results for resource-constrained countries where ARV treatment programs are being rolled out.

All of the published HIV transmission models of ARV resistance are based on simple biological assumptions and can track only one resistant strain (*3*–*8*). Our amplification cascade model captures biological complexity by generating a dynamic network composed of multiple ARV-resistant strains. We modeled the multistrain network in San Francisco by classifying ARV-resistant strains into seven categories; each category was defined based on the specific class of drugs to which the strain was resistant (NRTIs, NNRTIs, or PIs) and the level of resistance (single-, dual-, or triple-class) (Fig. 1A and fig. S1). Single-class resistance was to NRTIs, NNRTIs, or PIs. Dual-class resistance was to NRTIs and NNRTIs, NRTIs and PIs, or NRTIs and PIs. Triple-class resistance was to all three. Each class of ARVs contains several drugs (table S1) (*9*). In our modeling framework, if a strain is classified as resistant to a certain class of ARVs, then the strain is resistant to at least one drug in that class.

We modeled treatment effects by specifying treatment regimens and then assessing the effects of these regimens on infectivity and the probability of developing resistance. In the model, treated individuals receive a regimen to which their virus is sensitive; hence, we assume that treated individuals achieve either complete or partial viral suppression. We consider patients who achieve complete viral suppression to be noninfectious and incapable of developing resistance. Patients who achieve only partial viral suppression retain some degree of infectivity and are capable of developing resistant strains. When individuals experience treatment failure (which is usually determined by viral rebound), they can be switched to new drugs either in the same class or in a new class. For example, if a patient (in the model) is on a regimen containing zidovudine (NRTI), lamivudine (NRTI), and nelfinavir (PI) and develops resistance to nelfinavir, he could be switched to another PI (for example, indinavir). The model includes a matrix that specifies the rates at which strains develop resistance; therefore, strains are directly linked through the acquisition and amplification of resistance.

In the model, resistant and wild-type strains are assumed to compete to transmit HIV to uninfected at-risk MSM. These competitive interactions are mediated through strain-specific infectivity: The greater the infectivity, the higher the probability that the strain will be transmitted. We ascribe a competitive advantage to wild-type strains by assuming that they are always more infectious than the resistant strains. Furthermore, based on available competitive-fitness assays, replication-capacity assays, and patterns of developed resistance, we assume that the NNRTI-resistant strains are more transmissible than the NRTI-resistant strains, which, in turn, are more transmissible than the PI-resistant strains (*10*, *11*). In addition, we assume, based on the available data, that the transmissibility of virus strains decreases as the number of classes of resistance increases (*12*). Once an individual becomes infected with a wild-type or resistant strain, the model tracks viral dynamics, and consequently infectivity, through four stages of disease progression: (i) primary infection; (ii) not yet eligible for ARVs (that is, CD4 count > 350 cells/μl); (iii) eligible for ARVs (CD4 ≤ 350 cells/μl) but not currently undergoing ARV treatment; and (iv) ARV treatment. The 33 equations that specify the model, as well as a more detailed description of the structure, are given in (*9*). Parameter estimates are discussed in section 2 of (*9*), tables S2 to S11, and fig. S2. The model can be extended to include any number of additional drug classes, such as integrase inhibitors, co-receptor blockers, and fusion inhibitors, as they are introduced into new therapeutic regimens.

Before making predictions, we used the model (coupled with an uncertainty analysis) to reconstruct the evolution and transmission dynamics of the network of ARV-resistant strains (*13*). We calibrated the model, using Monte Carlo filtering techniques, to match the epidemiological conditions in San Francisco in 1987 when ARVs were first introduced [section 3 of (*9*)] (table S12). By the late 1980s, almost half of the MSM community was infected with HIV (*14*, *15*). After calibration, we used the model to simulate the evolutionary dynamics, from 1987 to 2008, of a network of ~4000 resistant strains, where each strain differed in drug susceptibility and infectivity. The history of ARV therapy in San Francisco can be divided into four eras spanning two decades

[1]Center for Biomedical Modeling, Semel Institute of Neuroscience & Human Behavior, David Geffen School of Medicine, University of California Los Angeles, Los Angeles, CA 90024, USA. [2]Department of Medicine AIDS Division, University of California San Francisco, San Francisco, CA 94110, USA.

*Present address: Department of Mathematics and Faculty of Medicine, University of Ottawa, Ottawa, K1N 6N5, Ontario, Canada.

†These authors contributed equally to this work.

‡Present address: Department of Mathematics, University of Tennessee, Knoxville, TN 37996, USA.

§To whom correspondence should be addressed. E-mail: sblower@mednet.ucla.edu

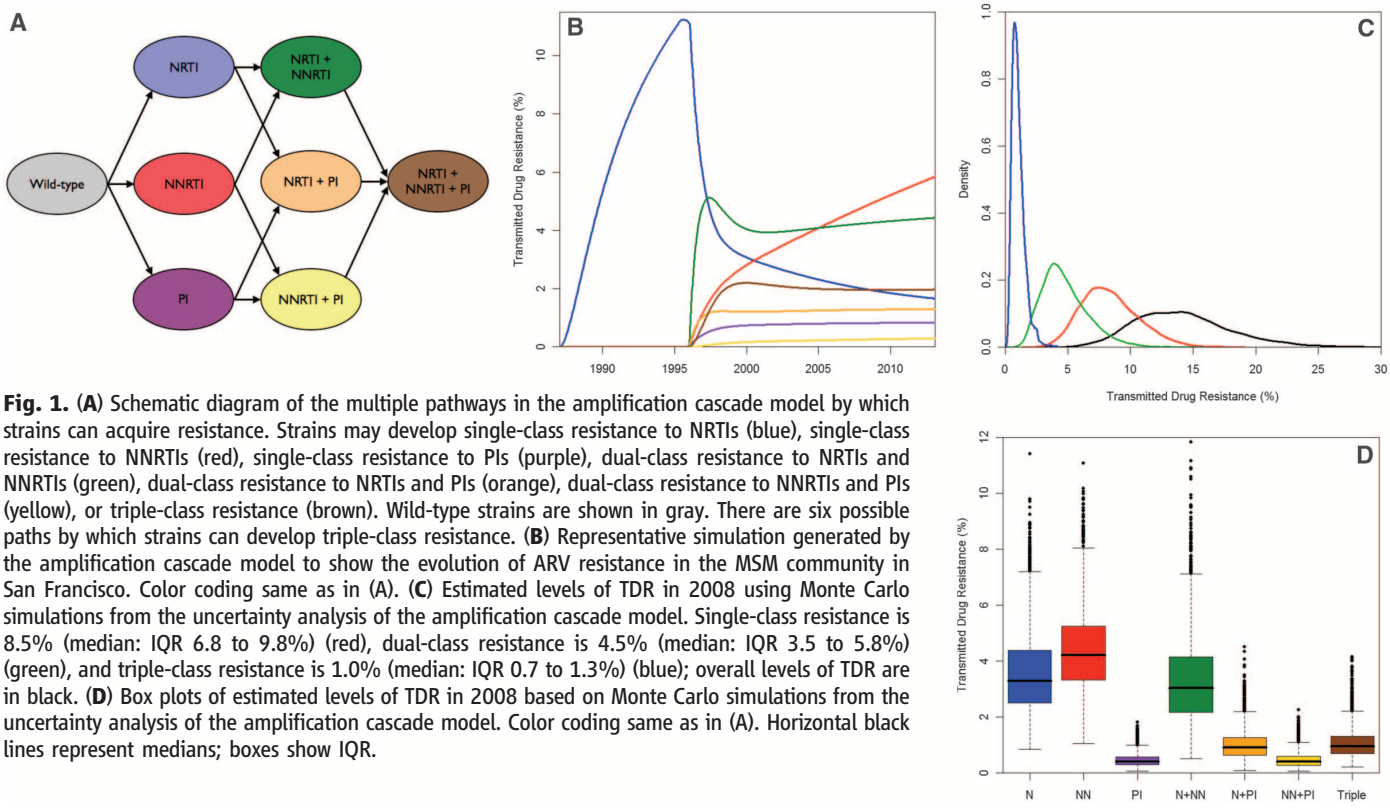

Fig. 1. (**A**) Schematic diagram of the multiple pathways in the amplification cascade model by which strains can acquire resistance. Strains may develop single-class resistance to NRTIs (blue), single-class resistance to NNRTIs (red), single-class resistance to PIs (purple), dual-class resistance to NRTIs and NNRTIs (green), dual-class resistance to NRTIs and PIs (orange), dual-class resistance to NNRTIs and PIs (yellow), or triple-class resistance (brown). Wild-type strains are shown in gray. There are six possible paths by which strains can develop triple-class resistance. (**B**) Representative simulation generated by the amplification cascade model to show the evolution of ARV resistance in the MSM community in San Francisco. Color coding same as in (A). (**C**) Estimated levels of TDR in 2008 using Monte Carlo simulations from the uncertainty analysis of the amplification cascade model. Single-class resistance is 8.5% (median: IQR 6.8 to 9.8%) (red), dual-class resistance is 4.5% (median: IQR 3.5 to 5.8%) (green), and triple-class resistance is 1.0% (median: IQR 0.7 to 1.3%) (blue); overall levels of TDR are in black. (**D**) Box plots of estimated levels of TDR in 2008 based on Monte Carlo simulations from the uncertainty analysis of the amplification cascade model. Color coding same as in (A). Horizontal black lines represent medians; boxes show IQR.

(*9*, *16*) (fig. S3 and table S1). Different regimens were used in each era. We modeled the specific regimens that were available in each era by using data on the proportion of patients achieving viral suppression (tables S6 to S9), degree of reduction in viral load in partially virally suppressed patients (tables S2 and S5), rate of development of resistance in treated patients (tables S6 to S9), and treatment-induced increase in survival time (table S10) (*9*). Because usage of ARVs has increased over the past two decades, we modeled era-specific treatment rates (table S4) (*9*).

The model reproduced and explained the observed evolutionary dynamics of the network of ARV-resistant strains over the four treatment eras (Fig. 1B). The first era began in 1987 when AZT (azidothymidine, an NRTI) was introduced as a monotherapy. AZT was used by a high proportion (36 to 68%) of MSM in San Francisco (*17*–*19*). Single-class resistance to NRTIs arose quickly (*1*), because they were ineffective at suppressing viral loads (*19*). In 1992, the second era began when dual therapies (based on two NRTIs) were introduced. These therapies were substantially more effective than monotherapies and achieved 30 to 60% viral suppression (*20*, *21*). Single-class resistance to NRTIs decreased, but dual-class resistance quickly developed, because many individuals had previously developed resistance to AZT. In 1996, the third era [early highly active antiretroviral therapy (HAART)] began when NNRTIs and PIs were used in triple-therapy regimens. Resistance to PIs was slow to emerge and has only risen to low levels, because multiple mutations are necessary to develop resistance to most drugs in this class (*22*). By 2001, more effective triple therapies (characterized by dual PIs combined with NRTIs) were developed, marking the beginning of the fourth era (modern HAART). During this recent era, the overall level of TDR appears to have stabilized (*2*); the model-generated network also exhibits this behavior (Fig. 1B). Recent empirical data from San Francisco indicate that transmission of single-class resistance is high, that of dual-class is moderate, and that of triple-class is low. In addition, studies indicate that transmission of NNRTI resistance is greater than that of NRTI resistance, which is greater than transmission of PI resistance. The model-generated transmission network shows these same patterns (Fig. 1, C and D). Our modeling estimates the overall level of TDR in 2008 to be 14% [median: interquartile range (IQR) 11.4 to 16.5%] (Fig. 1C), which is in extremely close agreement with empirically derived estimates of 13 to 16% (*2*).

After reconstructing the historical epidemiology up to 2008, we simulated the amplification cascade model for 5 more years to predict the levels of TDR in 2013. Our simulations revealed that resistance to single-class NRTIs and PIs will remain at current levels, but NNRTI resistance will increase (Fig. 2A). Regression analysis determined that the degree of increase in NNRTI resistance will depend ($P < 0.05$) on the proportion of patients who are infected with wild-type strains and are being treated with a regimen of two NRTIs and one NNRTI and who achieve viral suppression (Fig. 2B). This proportion depends on the efficacy of the regimen and adherence to it; thus, if only 70% are virally suppressed, NNRTI resistance could increase by more than 30% (Fig. 2B). This increase is predicted to be mainly due to transmission from untreated individuals infected with NNRTI-resistant strains who are in either the acute or chronic stage of infection.

The value of a strain's control reproduction number R_c specifies the average number, based on the probability that the individual is treated, of secondary HIV infections that an individual generates during their entire infectious period. R_c is a measure of a strain's transmission potential. A strain is capable of generating a self-sustaining epidemic if $R_c > 1$. The R_cs of the currently circulating ARV-resistant strains in San Francisco vary considerably (Fig. 3A). However, strains fall into three mutually exclusive groups (Fig. 3B) [section 4 of (*9*)]. Almost a quarter (24%) of the strains (Fig. 3B) cause less than one new infection ($R_c < 1$) and will eventually be eliminated (blue). Although other strains (Fig. 3B) also cause, on average, less than one new infection ($R_c < 1$), they will continue to be transmitted, because they evolve greater levels of resistance (green). We estimated that 60% of resistant strains have an $R_c > 1$ (Fig. 3B; red). Approximately 75% of these resistant strains have single-class resistance to NNRTIs, and 20% have dual-class resistance to NNRTIs and NRTIs. Although all have the potential to cause self-sustaining epidemics of resistance, they are all less infectious than the wild-type strains in San Francisco (Fig. 3C).

Similar trends for TDR to those observed in San Francisco and those predicted by our model have been documented in other cities in the

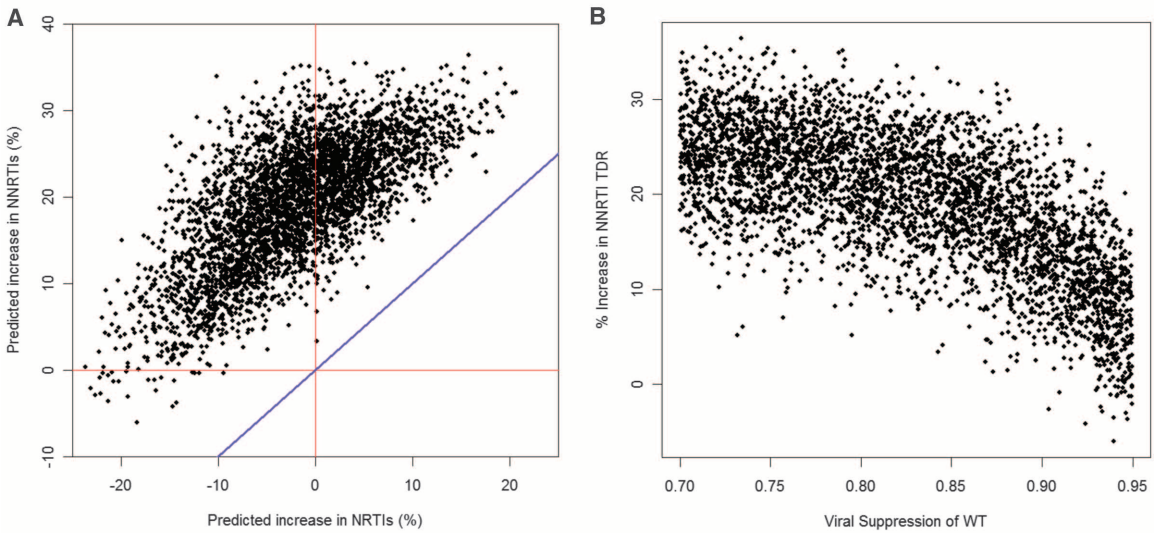

Fig. 2. (**A**) Predictions showing that transmission of strains that are resistant to NNRTIs will increase in San Francisco over the next 5 years. Predictions were made using Monte Carlo simulations from the uncertainty analysis of the amplification cascade model. Red lines show no increase in NNRTIs or NRTIs over the next 5 years. Blue line indicates an equal increase of NNRTIs and NRTIs over the next 5 years. (**B**) Predicted increase in the level of transmitted NNRTI resistance in San Francisco over the next 5 years as a function of the proportion of patients (who are infected with wild-type strains and are being treated with a regimen of two NRTIs and one NNRTI) who achieve viral suppression. Predictions were made using Monte Carlo simulations from the uncertainty analysis of the amplification cascade model.

United States and Europe that have analogous histories of ARV therapy. Potentially NNRTI-resistant strains similar to those we have identified in San Francisco may be increasing elsewhere. Although the NNRTI-resistant strains that we have identified are causing the rising wave of NNRTI resistance, they are unlikely to lead to self-sustaining epidemics in San Francisco or other communities in resource-rich countries, because new drugs will continue to become available. However our results may have important implications for HIV treatment programs in resource-constrained countries, where second-line regimens are not generally available. NNRTI-resistant strains are already evolving in many of these countries, because their first-line regimens are based on two NRTIs plus one NNRTI. Our current predictions have been obtained by modeling the evolution of resistance in individuals infected with subtype B strains. Subtype B accounts for ~12% of worldwide infections (and persons with subtype B are the most ARV-experienced), but 50% of prevalent HIV infections and 47% of all new HIV infections worldwide are caused by subtype C (*23*). Although information is limited, preliminary data suggest that treatment response and resistance patterns for subtype C are similar to those of subtype B (*24*). These data suggest that our results are likely to be generalizable to an epidemic of HIV-1 resistance among individuals infected with HIV-1 subtype C, and NNRTI-resistant strains with $R_c > 1$ could emerge in resource-constrained countries. If the R_c of the wild-type strains is reduced below one, as could occur by using a universal testing and treatment strategy (*25*), self-sustaining epidemics of NNRTI-resistant strains could arise (Fig. 3B and fig. S5) [section 5 of (*9*)].

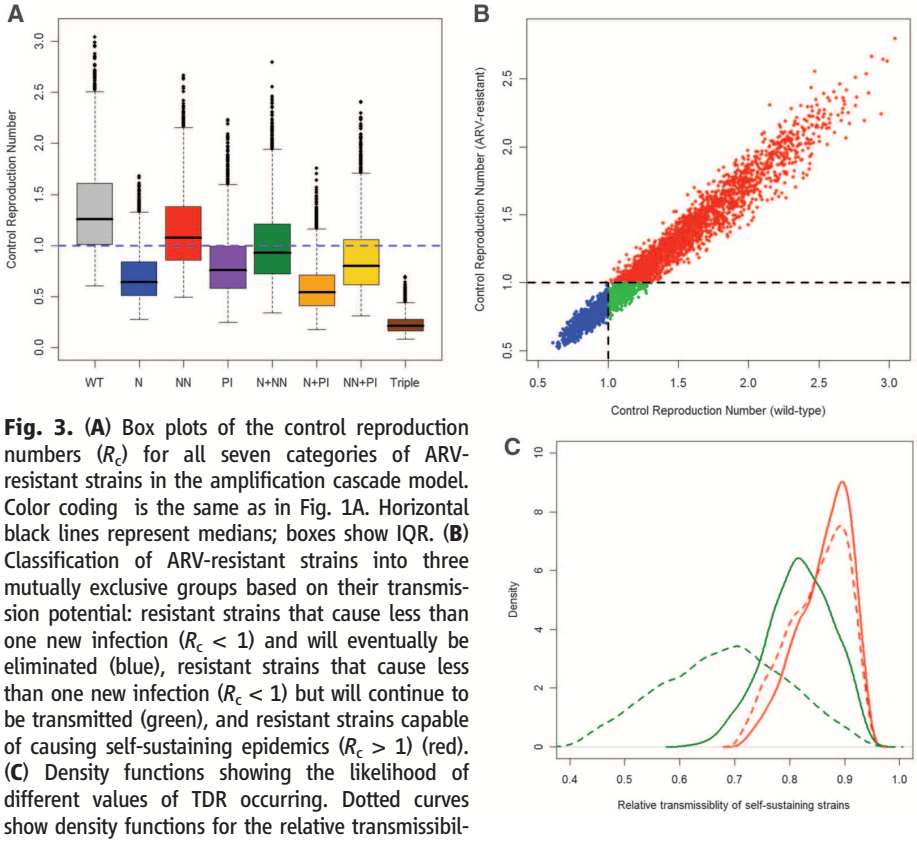

Fig. 3. (**A**) Box plots of the control reproduction numbers (R_c) for all seven categories of ARV-resistant strains in the amplification cascade model. Color coding is the same as in Fig. 1A. Horizontal black lines represent medians; boxes show IQR. (**B**) Classification of ARV-resistant strains into three mutually exclusive groups based on their transmission potential: resistant strains that cause less than one new infection ($R_c < 1$) and will eventually be eliminated (blue), resistant strains that cause less than one new infection ($R_c < 1$) but will continue to be transmitted (green), and resistant strains capable of causing self-sustaining epidemics ($R_c > 1$) (red). (**C**) Density functions showing the likelihood of different values of TDR occurring. Dotted curves show density functions for the relative transmissibility for all of the strains with single-class resistance to NNRTIs (red: median 86%, IQR 81 to 89%) and dual-class resistance to NRTIs and NNRTIs (green: median 69%, IQR 60 to 76%) that are circulating in the current network in San Francisco. Solid curves show density functions for the relative transmissibility of NNRTI-resistant strains with $R_c < 1$: single-class NNRTIs (red: median 87%, IQR 83 to 90%) and dual-class NRTIs and NNRTIs (green: median 82%, IQR 78 to 86%). Transmissibility is defined relative to the wild type.

Current levels of TDR, as well as the biological composition of the complex multistrain network, have emerged from two decades of treatment. To identify the key drivers of ARV resistance, we constructed classification and regression trees (CART) (*26*) using the 20-year data set (1987 to 2008) that was generated during the uncertainty analysis of the amplification cascade model. To build trees, we used the model's estimated level of TDR for 2008 as the response variable and the model's 50 parameters as predictor variables [section 6 of (*9*)]. The optimal tree revealed the hidden hierarchical structure of the data (Fig. 4). Key drivers of TDR are the predictor variables with

the highest importance scores (IS) (table S13) (*9*). The most important driver (IS = 100) is the average time (at the population level) it takes for CD4 cell counts in infected individuals to fall below 350 cells/μl (ν^{-1}) (Fig. 4). TDR was significantly higher (>15%) when CD4 counts fell to this threshold within ~6 years than when counts fell more gradually (Fig. 4 and fig. S6A) (*9*). This occurred because faster immunological deterioration led to increased treatment rates and accelerated the acquisition of resistance; hence, TDR increased as ν^{-1} decreased.

A high proportion of the transmission of wild-type strains over the past 20 years has occurred from asymptomatic individuals with a CD4 count > 350 cells/μl (fig. S6B) (*9*). Consequently, α_1^H, the infectiousness of strains in asymptomatic individuals, has been the second key driver of TDR (IS = 73) (Fig. 4); infectivity is defined in terms of the probability of transmitting HIV per sex act. These results can be understood in terms of classical competition theory (*27*): The most infectious wild-type strains had the greatest advantage over resistant strains and hence caused the lowest levels of TDR. A recent review of empirical estimates of the transmission probability per sex act indicates that α_1^H is likely to be greater than 0.0024 (*28*). The tree (Fig. 4) reveals that if wild-type strains had been less infectious (specifically, $\alpha_1^H \leq 0.0024$), it would have been very likely (probability 0.71) that TDR in San Francisco would be even higher than the current level (fig. S6C) (*9*).

We found α_1^T, the infectiousness of strains under treatment pressure, to be the third key driver of TDR (IS = 60) (Fig. 4). This driver represents the probability that an individual who is receiving current ARV regimens transmits HIV during one sex act. In contrast to our previous finding for α_1^H, TDR was significantly higher (>15%) when wild-type strains were more infectious ($\alpha_1^T > 0.0015$) than when they were less infectious ($\alpha_1^T \leq 0.0015$) (Fig. 4). This paradoxical result cannot be understood in terms of classical competition theory (*27*). It occurred because the effect of evolution on network dynamics was greater than that of competition. Under treatment pressure, the most infectious wild-type strains ($\alpha_1^T > 0.0015$) tended to evolve into the most infectious resistant strains; α_1^T only had a minor effect on competition, because treated individuals were relatively unimportant in transmitting wild-type strains (fig. S6D) (*9*). The value of α_1^T can be translated into viral load (fig. S2) [section 2 of (*9*)]; a value of 0.0015 corresponds to a viral load of 20,000 copies/ml. Effective therapies used in recent years have reduced viral loads in patients infected with wild-type strains to well below 20,000 copies/ml (*29*), indicating that α_1^T is (and was) significantly less than 0.0015. Given these effective treatments, our tree shows it is highly unlikely (probability 0.22) that TDR in San Francisco could have risen to more than 15% by 2008 (Fig. 4).

Our CART analysis also identified four other parameters that are important drivers of TDR, including the relative transmissibility of strains with single-class resistance to NRTIs (λ_2) (IS = 51), the degree of viral suppression in patients who are infected with wild-type strains and not completely virologically suppressed (γ_1) (IS = 45), the relative transmissibility of strains with dual-class resistance to NRTIs and NNRTIs (λ_5) (IS = 40), and finally the degree of viral suppression in patients who are infected with strains that have single-class resistance to NNRTIs and are not completely virologically suppressed (γ_3) (IS = 39). None of the 43 other predictor variables was found to be important (IS < 30). The tree shows that TDR has remained below 15% because of specific immunologic, virologic, and treatment factors operating in San Francisco (Fig. 4).

The amplification cascade model can be recalibrated and reparameterized to assess the dynamics of networks of ARV-resistant strains of HIV in any setting where ARVs are available. We have applied it to San Francisco. We have shown that a complex network of HIV strains has arisen in this city due to two decades of sequential selection for resistance; first with single agents, then dual agents, and, more recently, a combination of multiple-class agents. By designing a biologically complex multistrain network model, we have obtained important insights into the otherwise hidden dynamics of drug-resistant strains of HIV. We have identified the key immunological, virological, and treatment variables, as well as the hierarchical interactions among these variables, which have had a key role in driving resistance. Our results have shown that effective treatments have prevented TDR from increasing to greater than 15% in San Francisco. However, our modeling shows that the network is continuing to evolve. We found that the majority of the resistant strains currently being transmitted in this city are capable of causing self-sustaining epidemics, and we have estimated that an individual with an NNRTI-resistant strain can cause, on average, more than one new infection. We predict that a wave of NNRTI-resistant strains will emerge over the next 5 years in San Francisco due to transmission from untreated individuals. Our results also have implications for resource-constrained countries where first-line regimens are based on NNRTIs. If the resistant strains we have identified in our analyses evolve in these countries, they could substantially compromise HIV treatment programs. Consequently, current-

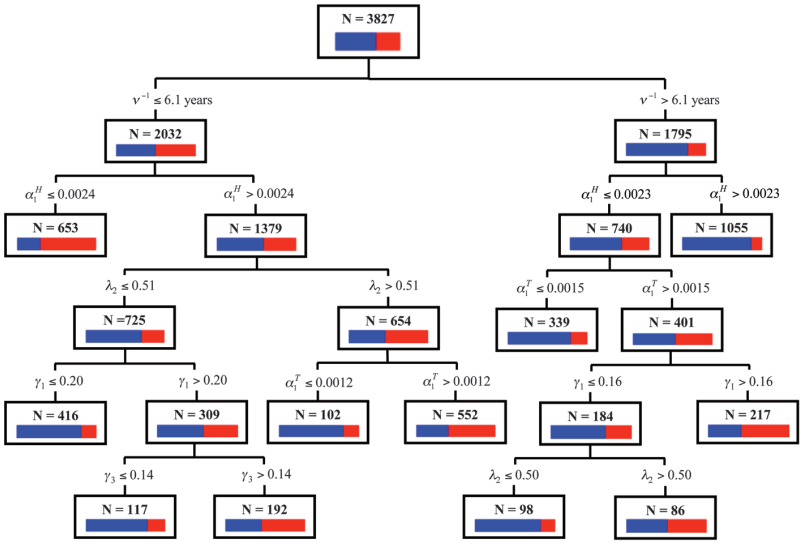

Fig. 4. A pruned version of the optimal tree. The root node contains data from the 3827 filtered Monte Carlo simulations that were generated by the amplification cascade model; filtered simulations are after model calibration [section 3 of (*9*)]. Inside each node is the total number of simulations it contains (N), as well as the distribution of the response variable TDR. Low levels of TDR (<15%) are blue, whereas high levels of TDR (>15%) are red. The most important variable (IS = 100) is ν^{-1}, the average time (at the population level) it takes for CD4 cell counts in infected individuals to fall below 350 cells/μl. The variable α_1^H reflects the degree of infectivity of wild-type strains during the asymptomatic stage of infection, where infectivity is specified as the probability of transmitting HIV during one sex act. The variable α_1^T represents the probability that an individual receiving a current ARV regimen transmits HIV during one sex act. The remaining variables are as follows: the transmissibility of strains (relative to the wild type) with single-class resistance to NRTIs (λ_2), the degree of viral suppression in patients who are infected with wild-type strain and are not completely virologically suppressed (γ_1), and the degree of viral suppression in patients who are infected with strains that have single-class resistance to NNRTIs and are not completely virologically suppressed (γ_3). Because the pruned tree is a subtree of the optimal tree, not every variable deemed important appears in it. The optimal tree has 84% predictive power in correctly identifying which simulations will generate high levels of TDR and 82% predictive power in correctly identifying which simulations will generate low levels of TDR.

ly circulating NNRTI-resistant strains in San Francisco pose a great and immediate threat to global public health.

References and Notes

1. B. A. Larder, G. Darby, D. D. Richman, *Science* **243**, 1731 (1989).
2. H. M. Truong *et al*., *AIDS* **20**, 2193 (2006).
3. S. M. Blower, H. B. Gershengorn, R. M. Grant, *Science* **287**, 650 (2000).
4. J. Goudsmit *et al*., *AIDS* **15**, 2293 (2001).
5. A. Phillips, *Nat. Med.* **7**, 993 (2001).
6. E. Tchetgen, E. H. Kaplan, G. H. Friedland, *J. Acquir. Immune Defic. Syndr.* **26**, 118 (2001).
7. R. Vardavas, S. Blower, J. J. Miranda, *PLoS ONE* **2**, e152 (2007).
8. G. S. Zaric, M. L. Brandeau, A. M. Bayoumi, D. K. Owens, *Simulation* **71**, 262 (1998).
9. Materials and methods are available as supporting material on *Science* Online.
10. C. L. Booth, A. M. Geretti, *J. Antimicrob. Chemother.* **59**, 1047 (2007).
11. J. Martinez-Picado, M. A. Martínez, *Virus Res.* **134**, 104 (2008).
12. L. Ross, N. Parkin, R. Lanier, *AIDS Res. Hum. Retroviruses* **24**, 617 (2008).
13. S. Blower, H. Dowlatabadi, *Int. Stat. Rev.* **62**, 229 (1994).
14. W. Lang *et al*., *JAMA* **257**, 326 (1987).
15. W. Winkelstein Jr. *et al*., *JAMA* **257**, 321 (1987).
16. J. K. Louie, L. C. Hsu, D. H. Osmond, M. H. Katz, S. K. Schwarcz, *J. Infect. Dis.* **186**, 1023 (2002).
17. W. Lang, D. Osmond, K. Page-Bodkin, A. Moss, W. Winkelstein Jr., *J. Acquir. Immune Defic. Syndr.* **6**, 191 (1993).
18. W. Lang *et al*., *J. Acquir. Immune Defic. Syndr.* **4**, 713 (1991).
19. J. C. Schmit *et al*., *AIDS* **12**, 2007 (1998).
20. J. J. Eron *et al*., *N. Engl. J. Med.* **333**, 1662 (1995).
21. C. Katlama *et al*., *JAMA* **276**, 118 (1996).
22. D. R. Kuritzkes, *AIDS Patient Care STDS* **18**, 259 (2004).
23. B. S. Taylor, M. E. Sobieszczyk, F. E. McCutchan, S. M. Hammer, *N. Engl. J. Med.* **358**, 1590 (2008).
24. A. J. Kandathil *et al*., *Indian J. Med. Microbiol.* **27**, 231 (2009).
25. R. M. Granich, C. F. Gilks, C. Dye, K. M. De Cock, B. G. Williams, *Lancet* **373**, 48 (2009).
26. L. Breiman, J. H. Freidman, R. A. Olshen, C. J. Stone, *Classification and Regression Trees* (Chapman & Hall, Boca Raton, FL, 1984).
27. C. Darwin, *The Origin of Species* (Signet, London, new ed. 1, 2003).
28. K. A. Powers, C. Poole, A. E. Pettifor, M. S. Cohen, *Lancet Infect. Dis.* **8**, 553 (2008).
29. S. M. Hammer *et al*., *JAMA* **300**, 555 (2008).

30. R.J.S., J.T.O., E.N.B., and S.B. acknowledge the financial support of the National Institute of Allergy and Infectious Diseases (NIAID) (RO1 AI041935). R.J.S. is supported by a Natural Sciences and Engineering Research Council of Canada discovery grant, an Early Researcher award, and funding from Mathematics of Information Technology and Complex Systems. In addition, S.B. acknowledges the John Simon Guggenheim Foundation, the National Academies Keck Foundation, and the Semel Institute for Neuroscience & Human Behavior. J.S.K. acknowledges NIAID grants P30-AI27763, NCRR K24RR024369, and AHRQ R18-HS017784. We thank R. Breban, D. Freimer, J. Freimer, N. Freimer, N. Jewell, E. Kajita, T. Pylko, V. Supervie, and R. Vardavas for useful discussions throughout the course of this research.

Supporting Online Material

www.sciencemag.org/cgi/content/full/science.1180556/DC1
Materials and Methods
Figs. S1 to S6
Tables S1 to S13
References

13 August 2009; accepted 16 December 2009
Published online 14 January 2010;
10.1126/science.1180556
Include this information when citing this paper.

Optimal Localization by Pointing Off Axis

Yossi Yovel,[1] Ben Falk,[2] Cynthia F. Moss,[2] Nachum Ulanovsky[1]*

Is centering a stimulus in the field of view an optimal strategy to localize and track it? We demonstrated, through experimental and computational studies, that the answer is no. We trained echolocating Egyptian fruit bats to localize a target in complete darkness, and we measured the directional aim of their sonar clicks. The bats did not center the sonar beam on the target, but instead pointed it off axis, accurately directing the maximum slope ("edge") of the beam onto the target. Information-theoretic calculations showed that using the maximum slope is optimal for localizing the target, at the cost of detection. We propose that the tradeoff between detection (optimized at stimulus peak) and localization (optimized at maximum slope) is fundamental to spatial localization and tracking accomplished through hearing, olfaction, and vision.

Most sensory systems allow some active control over the information acquired from the environment (*1*–*6*). Nowhere is this more evident than in echolocating bats (*4*, *7*–*10*), which control many aspects of their sonar signal design (*4*, *7*, *9*, *11*–*16*) and use returning echoes to orient and forage in the dark (*4*, *7*–*16*). We trained Egyptian fruit bats to fly in a large flight room and land on a spherical target while relying exclusively on sonar (*17*). The bats' three-dimensional (3D) position was measured with two infrared cameras, and the shape and direction of their sonar beam pattern were measured with a 20-microphone array (*17*) (Fig. 1, A to D, and movie S1).

At the beginning of each trial, the target was randomly repositioned. Subsequently, the bat searched for the target, approached it, and landed on it, either by a straight flight or a curved trajectory (Fig. 1C and fig. S1). Unlike microbats (microchiropteran bats), which emit laryngeal tonal calls, Egyptian fruit bats are megabats (megachiropteran bats) that produce very short (50- to 100-μs) impulse-like tongue clicks, with frequencies centered at 30 to 35 kHz (fig. S2). While flying, bats typically emitted pairs of clicks, with an ~20-ms interval within the click pair and an ~100-ms interval between the pairs (Fig. 1A and fig. S3) (*18*, *19*). The bats pointed their sonar beam toward the left or the right, in an alternating manner as follows: left→right→100-ms interval→right→left (Fig. 1D and movie S1).

We observed two different phases of behavior. During the first stage, the bats did not necessarily lock their click pairs onto the target, and the directions of clicks were widely distributed (the "unlocked" phase). At the final stage, the bats directed their sonar clicks so that the vector average of the pair of clicks pointed toward the target with accuracy better than 30° (*17*). We refer to this as the "locked" phase (Figs. 1E, arrows, and 2A, top, and fig. S1C). During this phase, 0.5 s before landing, 80% of the click pairs were locked with accuracy better than 15° (Fig. 2A, bottom, gray lines). In 10% of the trials, the bats locked onto the target with average accuracy better than 5°. The left-right orientation of the clicks in the locked phase implies that the bats did not direct the maximum intensity of the click toward the target, contradicting the common notion that bats steer their sonar beam in order to maximize the signal-to-noise ratio (SNR) of the echoes (*13*, *20*).

Another possible strategy would be for the bats to direct the maximal slope of the beam's emission curve toward the target, because this would maximize changes in reflected echo energy that result from changes in the relative position of the bat and the target. Plotting the directional span of the beams between the right and left maximum slope (green lines in Fig. 1, E and F, and fig. S1, C and D) showed that the bats consistently placed the maximum slope of their beams onto the target (Fig. 1F and fig. S1D; the top and bottom of the green lines are close to direction 0°). Next, we examined the population distribution of the directions of the beams' maximum intensity and maximum slope (Fig. 2, B and C, top two rows). Before locking, the bats directed their sonar beams over a wide range of angles, spanning >100° around the target (Fig. 2B, top). After locking, however, they clearly directed their beam so that the maximum slope of the intensity curve of the beam, and not its peak, was on the target (Fig. 2C, middle row). All six bats exhibited this behavior (fig. S4).

When the maximum slope of the beam is directed toward an object, any motion of the object relative to the bat will result in the largest possible change in echo intensity. The sign of the energy change (positive or negative) corresponds to the

[1]Department of Neurobiology, Weizmann Institute of Science, Rehovot 76100, Israel. [2]Department of Psychology, Institute for Systems Research and Neuroscience and Cognitive Science Program, University of Maryland, College Park, MD 20742, USA.

*To whom correspondence should be addressed. E-mail: nachum.ulanovsky@weizmann.ac.il